Minimal model of calcium dynamics in two heterogeneous coupled cells

Allanah Kenny[a,b], Michael J. Plank[b,c,*], Tim David[a]

[a] *Department of Mechanical Engineering, University of Canterbury, Christchurch 8140, New Zealand*
[b] *School of Mathematics and Statistics, University of Canterbury, Christchurch 8140, New Zealand*
[c] *Te Pūnaha Matatini, Centre of Research Excellence, New Zealand*

Abstract

Intercellular calcium (Ca^{2+}) waves are an important signalling mechanism in a wide variety of cells within the body, crucial for cellular coordination and control. In order to investigate calcium dynamics in coupled cells, a minimal model describing intracellular Ca^{2+} dynamics in a single cell is extended to describe two adjacent cells coupled by a flux of Ca^{2+} via gap junctions. The Ca^{2+} dynamics of the single cell system are either excitable, nonexcitable or oscillatory, depending on the strength of external stimulus to the inositol trisphosphate (IP_3) dependent Ca^{2+} release pathway. We investigate how the stability and asymptotic dynamics of a system of two heterogeneous cells depend on the single-cell dynamics and the coupling strength. We show analytically that, in the case of very strong coupling, the asymptotic dynamics are the same as in a single cell whose IP_3 stimulus strength is the average of the two coupled cells. In cases where one or both cells have an unstable steady state when uncoupled, coupling causes a qualitative change in behaviour. This can include amplitude-modulated oscillations, mixed mode oscillations, and the coalescence of multiple frequencies as the cells eventually become synchronised.

Keywords: calcium-induced calcium release, coupled oscillator, gap junctions, intercellular signalling

*Corresponding author
Email address: michael.plank@canterbury.ac.nz (Michael J. Plank)

1. Introduction

Calcium (Ca^{2+}) is an important signalling messenger in a wide variety of cells [1–3]. Many cell types exhibit Ca^{2+} oscillations or Ca^{2+} spikes in response to external stimulation [4–7]. This can be in the form of excitable behaviour, meaning that a small stimulus does not produce a Ca^{2+} spike, but a sufficiently large stimulus can lead to a spike [8]. When a population of cells exhibits excitable behaviour or Ca^{2+} oscillations, they may be able to support a travelling wave of Ca^{2+} propagating through the cell population. Travelling Ca^{2+} waves have been documented in several cell types including hepatocytes [9, 10], epithelial cells [11], astrocytes [12], pancreatic beta cells [13] and pancreatic acinar cells [14]. There are two possible mechanisms for generation of a propagating Ca^{2+} wave: gap junctions that allow Ca^{2+} or other cytoplasmic messengers such as inositol trisphosphate (IP_3) to move directly between the cytosols of adjacent cells; and the release of diffusible paracrine messengers into the extracellular space [5, 12, 15].

There is evidence that intercellular signalling via propagating Ca^{2+} waves is a crucial means of cellular coordination and control [4, 16]. For example, smooth muscle cells (SMC), which line the arterial wall and effectively control the local supply of oxygen and glucose necessary for cellular function, are known to support travelling Ca^{2+} waves [17, 18]. Experimental studies have shown that synchronised Ca^{2+} oscillations in a population of SMC will induce vasomotion, the rhythmic dilation and contraction of the blood vessel wall [19–21]. Propagating Ca^{2+} waves may play a role in pathologies associated with impaired functional hyperaemia such as cortical spreading depression, migraine, and stroke [22].

In order to analyse the underlying dynamics of coupled cells, a possible starting point is to examine the Ca^{2+} dynamics of a single cell. There are many mathematical models of Ca^{2+} dynamics, ranging in complexity. Minimal models aim to reproduce observed phenomena, such as sustained Ca^{2+} oscillations, on a qualitative level with the minimum number of variables and channels [5]. Examples of minimal models describing the dynamics of cytosolic Ca^{2+} based on IP_3-initiated Ca^{2+} release from intracellular stores include [23–28]. More complex models include greater detail of the cellular physiology, such as the calcium channel

gating characteristics [29], the nonlinear interaction of membrane potential and intracellular calcium [30], coupled Ca^{2+} dynamics in different cell types [16], and stochastic effects [31–33]. For a review of different types of Ca^{2+} dynamics in single cells, see [34]. Phase-difference approximations can be used to describe the dynamics of pairs of electrically coupled neural oscillators, such as the Fitzhugh-Nagumo equations or Morris-Lecar model [33, 35, 36], but this approximation is only valid for weak coupling. Synchronisation of Ca^{2+} dynamics in systems of two coupled cell models has also been studied in [37–41].

Here, we focus on a minimal model of intracellular Ca^{2+} dynamics based on Ca^{2+}-induced Ca^{2+} release (CICR) from an intracellular Ca^{2+} store via a combination of IP_3-sensitive and IP_3-insensitive channels [24]. The model, which is described in Sec. 2.1, is for a non-electrically excitable cell and does not include membrane potential or fluxes of any second messengers other than Ca^{2+}. The Ca^{2+} dynamics are either excitable, nonexcitable or oscillatory, depending on the strength of external stimulus to the IP_3 dependent Ca^{2+} release pathway, which is treated as a bifurcation parameter. The simplicity of the model, although not quantitatively realistic, is advantageous because it allows analytical insight into the simplest possible mechanism that can generate synchronous or asynchronous Ca^{2+} oscillations in coupled cells.

In this paper, we extend the minimal Ca^{2+} model of [24] to describe a system of two cells with different IP_3 stimulus levels, coupled via Ca^{2+} gap junctions (Sec 2.2). We then investigate how the stability and asymptotic dynamics depend on the single-cell dynamics and the coupling strength. We derive analytical results for the asymptotic dynamics in the limiting case of strong coupling (Sec 3.1). We then use numerical solutions and spectral analysis to investigate qualitative changes in the dynamics of two heterogeneous cells as the coupling strengths changes. This numerical analysis is split into two cases: a system of two oscillatory cells (Sec. 3.2) and a system of one oscillatory and one excitable cell (Sec 3.3). Many previous analyses have focused on systems of coupled cells that are identical in their dynamics and only differ in their initial condition or have asymmetric coupling [36, 42–45]. Our results differ from these by analysing the Ca^{2+} dynamics in heterogeneous

cells and how these vary with coupling strength from zero coupling through to the strong coupling limit. Although we use a very simplified model of Ca^{2+} dynamics, its cubic nullclines and bifurcation structure are similar to or contained within those of some more complex models [33]. Therefore, our results give broad qualitative insights into potential mechanisms underlying intercellular Ca^{2+} communication (Sec. 4).

2. Methods

2.1. Single cell model

The minimal model [24] is composed of two state variables, the cytosolic Ca^{2+} concentration z and the Ca^{2+} concentration y in the IP_3-insensitive Ca^{2+} pool, referred to as the internal Ca^{2+} store. The dynamics are governed by differential equations for z and y:

$$\frac{dz}{dt} = v_0 + v_1\beta - v_2(z) + v_3(z,y) + k_f y - kz, \tag{1}$$

$$\frac{dy}{dt} = v_2(z) - v_3(z,y) - k_f y. \tag{2}$$

The terms v_0 and kz relate, respectively, to the flux of Ca^{2+} into and out of the cell. The term $k_f y$ refers to a nonactivated, leaky transport of Ca^{2+} from the internal (IP_3-insensitive) store to the cytosol and the term $v_1\beta$ refers to the flux of Ca^{2+} from the IP_3-sensitive pool. The terms v_2 and v_3 are the rate of Ca^{2+} pumping into the internal store and release from the internal store, respectively, and are given by the algebraic equations

$$v_2(z) = V_{M2}\frac{z^n}{K_2^n + z^n}, \tag{3}$$

$$v_3(z,y) = V_{M3}\frac{y^m}{K_R^m + y^m}\frac{z^p}{K_A^p + z^p}, \tag{4}$$

where V_{M2} and V_{M3} denote respectively the maximum rates of Ca^{2+} pumping into and release from the intracellular store. These rates are described by Hill functions with cooperativity coefficients n and m, respectively. The parameter p denotes the degree of cooperativity of the activation process.

When the cell receives an external signal via binding of an agonist, such as adenosine triphosphate (ATP), it triggers an increase in IP_3 [46]. This is implicitly modelled by an

Parameter	Value	Unit	Description
β	0 to 1		Saturation constant of the IP_3 receptor
v_0	1	μM s^{-1}	Ca^{2+} influx into the cell
k	10	s^{-1}	Rate of Ca^{2+} efflux out of the cell
k_f	1	s^{-1}	Rate of nonactivated, leaky transport from the IP_3-insensitive Ca^{2+} store
v_1	7.3	μM s^{-1}	Rate of Ca^{2+} influx from the IP_3-sensitive pool
V_{M2}	65	μM s^{-1}	Maximum rate of Ca^{2+} pumping into the IP_3-insensitive Ca^{2+} store
V_{M3}	500	μM s^{-1}	Maximum rate of Ca^{2+} release from the IP_3-insensitive Ca^{2+} store
K_2	1	μM	Pumping threshold constant
K_R	2	μM	Release threshold constant
K_A	0.9	μM	Activation threshold constant
n		2	Pumping cooperativity coefficient
m		2	Release cooperativity coefficient
p		4	Activation cooperativity coefficient

Table 1: Model parameters and values, taken from [24].

increase in the saturation constant β, which in turn leads to a rise in cytosolic Ca^{2+} concentration. The parameter β thus represents the strength of external stimulus to the IP_3 pathway, and may be varied between 0 and 1. We treat β as a bifurcation parameter. The other parameter values are taken from [24] and are listed in Table 1.

We non-dimensionalise the system by defining the following parameters and variables:

$$\bar{t} = k_f t,\ Z = \frac{k_f}{v_0} z,\ Y = \frac{k_f}{v_0} y,$$
$$\overline{v_1} = \frac{v_1}{v_0},\ \overline{V_{M2}} = \frac{V_{M2}}{v_0},\ \overline{V_{M3}} = \frac{V_{M3}}{v_0}, \overline{k} = \frac{k}{k_f},\ \overline{K_2} = \frac{k_f K_2}{v_0},\ \overline{K_R} = \frac{k_f K_R}{v_0},\ \overline{K_A} = \frac{k_f K_A}{v_0}.$$

Dropping the overbars, the system becomes

$$\frac{dZ}{dt} = 1 + v_1\beta - v_2(Z) + v_3(Z,Y) + Y - kZ, \tag{5}$$
$$\frac{dY}{dt} = v_2(Z) - v_3(Z,Y) - Y, \tag{6}$$

where

$$v_2(Z) = V_{M2}\frac{Z^n}{K_2^n + Z^n}, \tag{7}$$
$$v_3(Z,Y) = V_{M3}\frac{Y^m}{K_R^m + Y^m}\frac{Z^p}{K_A^p + Z^p}. \tag{8}$$

2.2. Coupled cell model

For the coupled cell model, we consider two adjacent cells coupled by Ca^{2+} gap junctions, modelled in a similar manner to previous studies [10, 47]. We use Z_i and Y_i to denote the Ca^{2+} concentrations in the cytosol and the internal store, respectively, and β_i to denote the saturation constant for cell i ($i = 1, 2$). All other parameters are assumed to take the same value for both cells.

We assume that transport of Ca^{2+} between the cells is linearly proportional to the difference in Ca^{2+} concentrations between the cytosol of the two cells. This is a simple, Fickian diffusion mechanism that ignores voltage-and concentration-dependence in the gap junction permeability and any voltage-dependent effects on the transport of charged ions [48]. A more complex coupling method used widely in cell modelling is the Goldman–Hodgkin–Katz (GHK) equation, which calculates the ionic exchange based on the electrochemical gradient from a variety of ions present in the cells [21, 49]. Nevertheless, there are a large number of modelling studies that have assumed a simple linear gap junction coupling [10, 50, 51].

The transport term introduces a new parameter d, which represents the permeability of the gap junctions. We refer to d as the coupling strength, with units of s^{-1}. To obtain an approximate value for d, we note that linear coupling of adjacent cells within a large population corresponds to Fickian diffusion of Ca^{2+} with diffusivity $P = dh^2$, where h is the length of a single cell [52]. We take h to be a typical cell length of approximately 50 μm. The diffusivity of free, extracellular Ca^{2+} is of the order 10^5 μm^2 s^{-1} [53], which corresponds to $d = 40$ s^{-1}. Intercellular transport of Ca^{2+} via gap junctions is likely to be much slower than this, but the precise value of the effective diffusivity P is not known. We therefore consider a range of values for $d = P/h^2$. In the special case where $d = 0$, then there is no coupling and the cells behave independently.

To non-dimensionalise the coupled cell system we define $D = \frac{d}{k_f}$. The non-dimensionalised

differential equations for the coupled system are:

$$\frac{dZ_1}{dt} = 1 + v_1\beta_1 - v_2(Z_1) + v_3(Z_1, Y_1) + Y_1 - kZ_1 + D(Z_2 - Z_1), \quad (9)$$

$$\frac{dZ_2}{dt} = 1 + v_1\beta_2 - v_2(Z_2) + v_3(Z_2, Y_2) + Y_2 - kZ_2 + D(Z_1 - Z_2), \quad (10)$$

$$\frac{dY_1}{dt} = v_2(Z_1) - v_3(Z_1, Y_1) - Y_1, \quad (11)$$

$$\frac{dY_2}{dt} = v_2(Z_2) - v_3(Z_2, Y_2) - Y_2, \quad (12)$$

There is no coupling term in the equations for Ca^{2+} in the internal store (Y_1 and Y_2) because this is an internal compartment within the cell, whereas the gap junctions are isolated to the cell membrane. The coupled cell system, Eqs. (9)–(12), is solved in Matlab using the *ode45* solver.

3. Results

Before presenting results for the coupled system of two cells, we briefly review the behaviour of the single cell model in Eqs. (5)–(8). A steady state of this dynamical system must satisfy:

$$0 = 1 + v_1\beta - kZ, \quad (13)$$

$$0 = Y^{m+1} + \left(V_{M3}\frac{Z^p}{K_A^p + Z^p} - V_{M2}\frac{Z^n}{K_2^n + Z^n} \right) Y^m + K_R^m Y - V_{M2}\frac{Z^n}{K_2^n + Z^n}. \quad (14)$$

Eq. (13) clearly has a unique solution $Z^* = (1 + v_1\beta)/k$. Eq. (14) has been obtained from Eq. (6) by multiplying both sides by $K_R^m + Y^m$ to obtain a polynomial in Y. It is straightforward to show that, for the parameter values considered (see Table 1), Eq. (14) is a cubic with exactly one non-negative root, which we will write as $Y^* = f(Z^*)$, noting that the function f is independent of β. Hence, the system has a unique steady state (Z^*, Y^*) for any value of β. The Jacobian matrix for the system is

$$J(Z, Y) = \begin{bmatrix} a(Z,Y) - k & b(Z,Y) \\ -a(Z,Y) & -b(Z,Y) \end{bmatrix},$$

where $a(Z, Y) = \partial/\partial Z(-v_2 + v_3)$ and $b(Z, Y) = 1 + \partial v_3/\partial Y$. The determinant of this matrix is $kb(Z, Y)$, which is always positive. This implies that the steady state is stable if and only

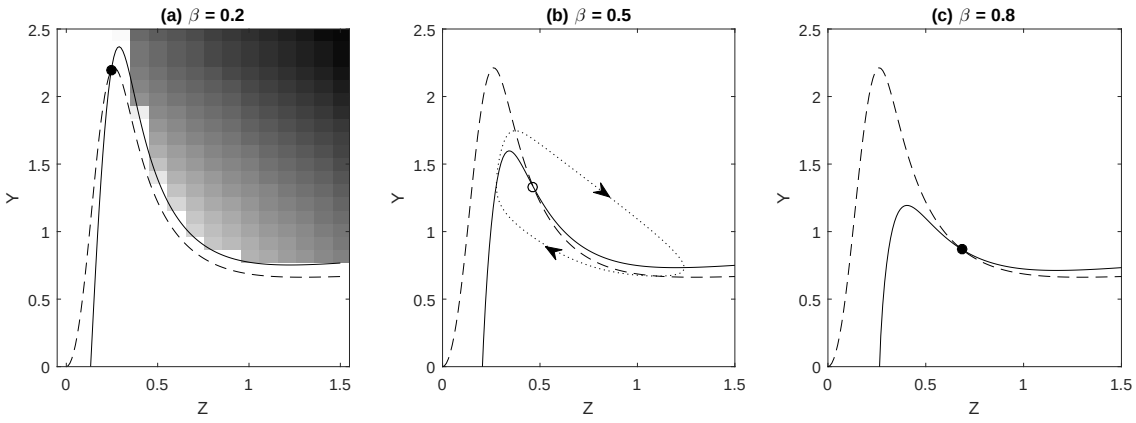

Figure 1: Phase space of the single-cell model in Eqs. (5)–(8) for three different values of the bifurcation parameter: (a) $\beta = 0.2$, the steady state is stable but the system is excitable meaning that a small perturbation from the steady state can result in a large excursion in phase space; (b) $\beta = 0.5$, the steady state is unstable and there is a stable limit cycle corresponding to sustained calcium oscillations; (c) $\beta = 0.8$, the steady state is stable and the system is not excitable. Graphs show the nullclines $dZ/dt = 0$ (solid) and $dY/dt = 0$ (dashed), steady state (stable = filled circle, unstable = open circle) and stable limit cycle (dotted). In (a), each pixel is shaded according to the maximum value of Z to which the trajectory increases, after starting from an initial condition at the location of the pixel: dark regions correspond to initial conditions that lead to a large excursion before returning to the steady state. Other parameter values as shown in Table 1.

if the trace of $J(Z^*, Y^*)$ is negative, and the only possible type of bifurcation of the steady state is a Hopf bifurcation, which occurs when the trace of $J(Z^*, Y^*)$ changes sign.

Figure 1 shows the phase portrait of the single cell model for three different values of the bifurcation parameter β and Figure 2 shows the bifurcation diagram. When β is small (Fig. 1(a)), the steady state is stable. However, initial conditions that are shaded dark grey in Fig. 1(a) lead to a large excursion in phase space (i.e. a Ca^{2+} spike) before returning to the steady state [54]. The boundary between the light and dark shaded regions in Fig. 1(a) is the excitability threshold. As β increases, the steady state moves closer to the turning point of the Z-nullcline. This means that the size of perturbation required to cause a Ca^{2+} spike is smaller, i.e. the cell becomes more excitable. At $\beta \approx 0.29$, there is a Hopf bifurcation (Fig. 2), resulting in loss of stability of the steady state and creation of a stable limit cycle (Fig. 1(b)). At $\beta \approx 0.77$, there is another Hopf bifurcation resulting in the steady state regaining stability and the limit cycle being destroyed. For $\beta > 0.77$, all trajectories tend to the stable steady state and the cell is no longer excitable (Fig. 1(c)).

We now turn to the two cell model in Eqs. (9)–(12), with non-dimensional coupling

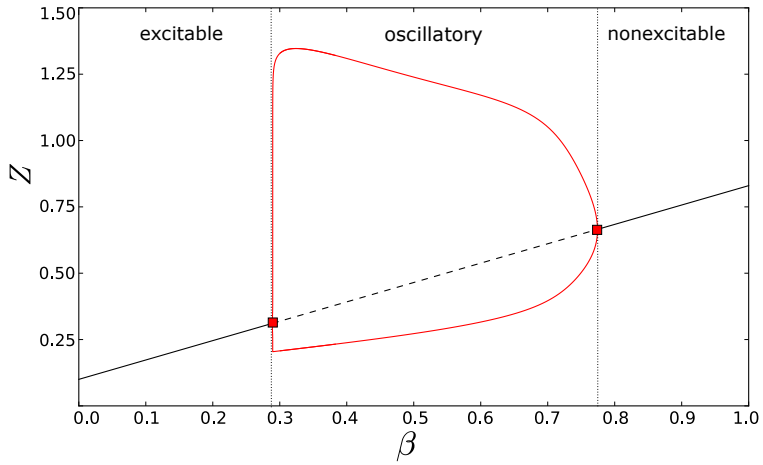

Figure 2: Bifurcation diagram for the single cell model in Eqs. (5)–(8) with β varied, showing the Hopf bifurcations (filled squares), stable steady state (solid black), unstable steady state (dashed black) and stable limit cycle (solid red). The dynamics are excitable for $\beta < 0.29$, oscillatory for $0.29 < \beta < 0.77$ and non-excitable for $\beta > 0.77$. Other parameter values as shown in Table 1.

strength D and bifurcation parameters β_1 and β_2. We focus on the long-term behaviour of the cells, i.e. after the transient effect of initial conditions. Transient behaviour may be biologically relevant in some situations, for example when there are fast and slow timescales [55]. However, under the present model, the cells typically converge onto an attractor (either a steady state or a limit cycle) within a few seconds, so studying long-term behaviour is reasonable.

3.1. Steady state and stability analysis

In this section, we will use (Z_i^*, Y_i^*) to denote the steady state of a single, uncoupled cell with $\beta = \beta_i$, and (Z_i, Y_i) to denote the coupled cell system. The steady state conditions for the coupled cell system are:

$$0 = 1 + v_1\beta_i - kZ_i + D(Z_j - Z_i), \tag{15}$$

$$Y_i = f(Z_i), \tag{16}$$

for $i = 1, 2$, $j \neq i$, and where $f(Z)$ denotes the root of Eq. (14), as in the single cell case. Straightforward algebra shows that this system has a unique steady state given by

$$Z_1 = \bar{Z}^* - \frac{k}{k+2D}\Delta Z^*, \tag{17}$$

$$Z_2 = \bar{Z}^* + \frac{k}{k+2D}\Delta Z^*, \tag{18}$$

and $Y_i = f(Z_i)$, where $\bar{Z}^* = (Z_1^* + Z_2^*)/2$ is the mean of the steady states for cell 1 and cell 2 when uncoupled and $2\Delta Z^* = Z_2^* - Z_1^*$ is the difference between the uncoupled steady states.

The stability of the steady state of the coupled system is determined by the 4×4 Jacobian matrix J, which can be written in block form as:

$$\begin{bmatrix} J(Z_1, Y_1) - D_M & D_M \\ D_M & J(Z_2, Y_2) - D_M \end{bmatrix}, \qquad \text{where } D_M = \begin{bmatrix} D & 0 \\ 0 & 0 \end{bmatrix}.$$

In the case of two identical cells ($\beta_1 = \beta_2$), the steady state is the same as in the uncoupled case (Z^*, Y^*), for any coupling strength D. The matrices $J(Z_1, Y_1)$ and $J(Z_2, Y_2)$ are both equal to $J(Z^*, Y^*)$. Hence, the eigenvalues of the 4×4 Jacobian are given by the two eigenvalues of $J(Z^*, Y^*)$, together with the two eigenvalues of $J(Z^*, Y^*) - 2D_M$. The trace of $J(Z^*, Y^*) - 2D_M$ is clearly less than the trace of $J(Z^*, Y^*)$, and the determinant of $J(Z^*, Y^*) - 2D_M$ is positive. Hence, the stability of the steady state is always the same as that of the uncoupled steady state, regardless of coupling strength D.

When the cells are non-identical ($\beta_1 \neq \beta_2$), Eqs. (17) and (18) show that as D increases, the steady state approaches the mean of the uncoupled steady states $(\bar{Z}^*, \bar{Y}^*)$. Since the steady state value of Z is linear in β (see Eq. (13)), this steady state is equal to that of a single cell with the average of the two coupled cells' values of the bifurcation parameter, $\bar{\beta} = (\beta_1 + \beta_2)/2$. When coupling is strong (large D), the matrices $J(Z_1, Y_1)$ and $J(Z_2, Y_2)$ are both approximately equal to $J(\bar{Z}^*, \bar{Y}^*)$. Hence, via the same argument as above for identical cells, the stability of the steady state in the strong coupling limit ($D \to \infty$) is the same as that of a single cell with $\beta = \bar{\beta}$.

We test the stability of the coupled system for intermediate coupling strengths with numerical calculations of the eigenvalues of the 4×4 Jacobian matrix evaluated at the steady state given by Eqs. (17) and (18). Figure 3 shows two-parameter bifurcation diagrams in the (β_1, β_2) space for four different coupling strengths. In the uncoupled case, stability is simply determined by the behaviour of the individual cells: the system as a whole is stable if and only if both individual cell steady states are stable (Fig. 3(a)). Increasing the coupling strength stabilises systems where one cell is excitable ($\beta_i < 0.29$) and the other is oscillatory

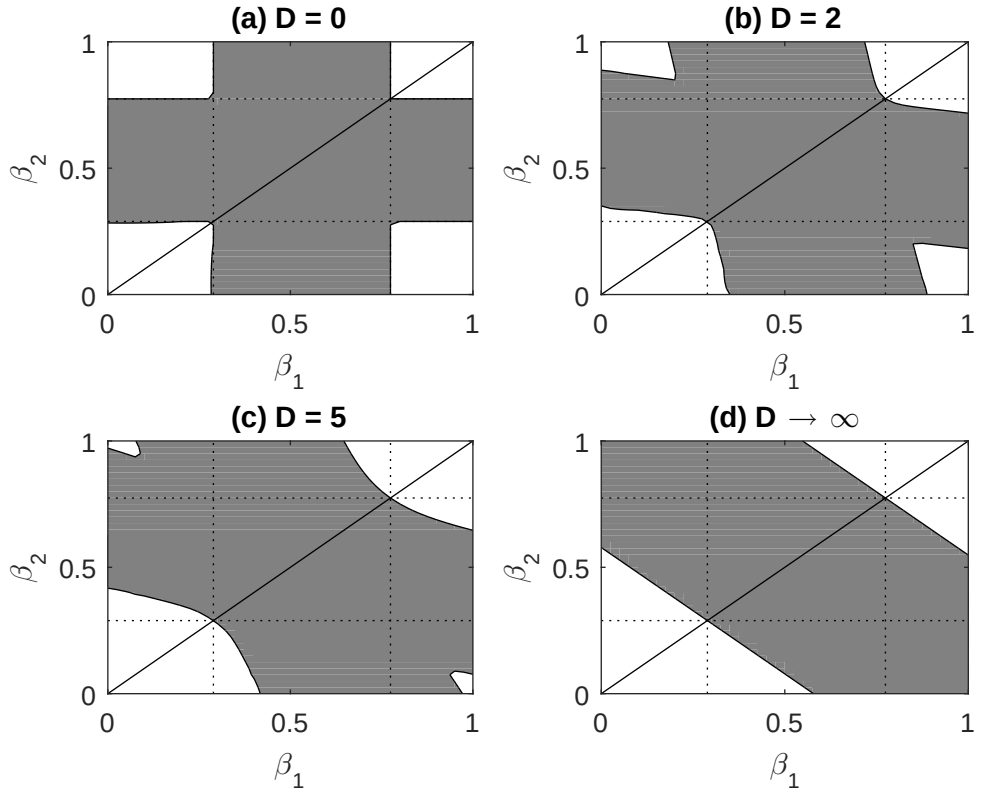

Figure 3: Two-parameter bifurcation diagrams for two cells: (a) uncoupled ($D = 0$); (b) coupled with $D = 2$; (c) coupled with $D = 5$; (d) in the strong coupling limit ($D \to \infty$). Light and dark regions respectively show combinations of the two cells' bifurcation parameters β_1 and β_2 for which the steady state is stable and unstable. In (a)–(c), stability is determined by calculating the dominant eigenvalue of the 4×4 Jacobian matrix evaluated at the steady state given by Eqs. (17) and (18). In (d), stability is determined by numerically calculating the dominant eigenvalue of the 2×2 Jacobian matrix evaluated at the steady state of a single cell with $\bar{\beta} = (\beta_1 + \beta_2)/2$. Solid diagonal line corresponds to identical coupled cells ($\beta_1 = \beta_2$). Dashed horizontal/vertical lines show the locations of the Hopf bifurcations in the single-cell system at $\beta = 0.29$ and $\beta = 0.77$. Other parameter values as shown in Table 1.

but close to the Hopf bifurcation ($\beta_j > 0.29$), and destabilises systems where one cell is excitable ($\beta_i < 0.29$) and the other is non-excitable ($\beta_i > 0.77$) (Fig. 3(b-c)). In the strong coupling limit, stability is determined by the behaviour of the a single cell with the average of two cells' values of β (Fig. 3(d)). Note that for coupled identical cells (diagonal lines in Fig. 3), the stability of the coupled system is always the same as that of a single cell, regardless of the coupling strength D.

These results establish the unique steady state and its stability for a pair of coupled cells. When the steady state is stable, it is possible that other non-equilibrium attractors, such as a stable limit cycle, could arise as a consequence of coupling. However, numerical explorations with varying initial conditions have shown no evidence of any bistability. Thus, when two excitable cells are coupled ($\beta_1, \beta_2 < 0.29$ in Fig. 3), the result is always convergence to the stable steady state. For the remainder of the paper, we focus on two representative cases where the steady state is unstable: coupling two oscillatory cells and coupling an oscillatory and an excitable cell.

3.2. Coupling two oscillatory cells

Figure 4 shows attractors for two coupled oscillatory cells, with $\beta_1 = 0.4$ and $\beta_2 = 0.5$, for a range of values of the coupling strength D. When uncoupled ($D = 0$), the cells oscillate independently, with different amplitudes and frequencies due to their different values of β. The time series of the uncoupled cells is shown in Fig. 5(a). When coupled ($D > 0$), the flux of Ca^{2+} between cells affects the oscillations, causing both cells to oscillate with variable amplitude (i.e. amplitude-modulated oscillations). This can be seen as cycles of different amplitude within the trajectories with $D > 0$ (Fig. 4), and in the time series shown in Fig. 5(b) for $D = 1$. As the coupling strength D increases, the intercellular flux of Ca^{2+} becomes larger. Eventually, when the coupling strength is above around $D = 2$, the cells synchronise and oscillate with a common frequency. There is a phase lag between the two cells (see Fig. 5(c) for example). In general, we use the term synchronisation to include phase-lagged oscillation at a common frequency. The phase lag becomes gradually smaller as D increases further, although fully in-phase synchronisation requires a value of D much higher than

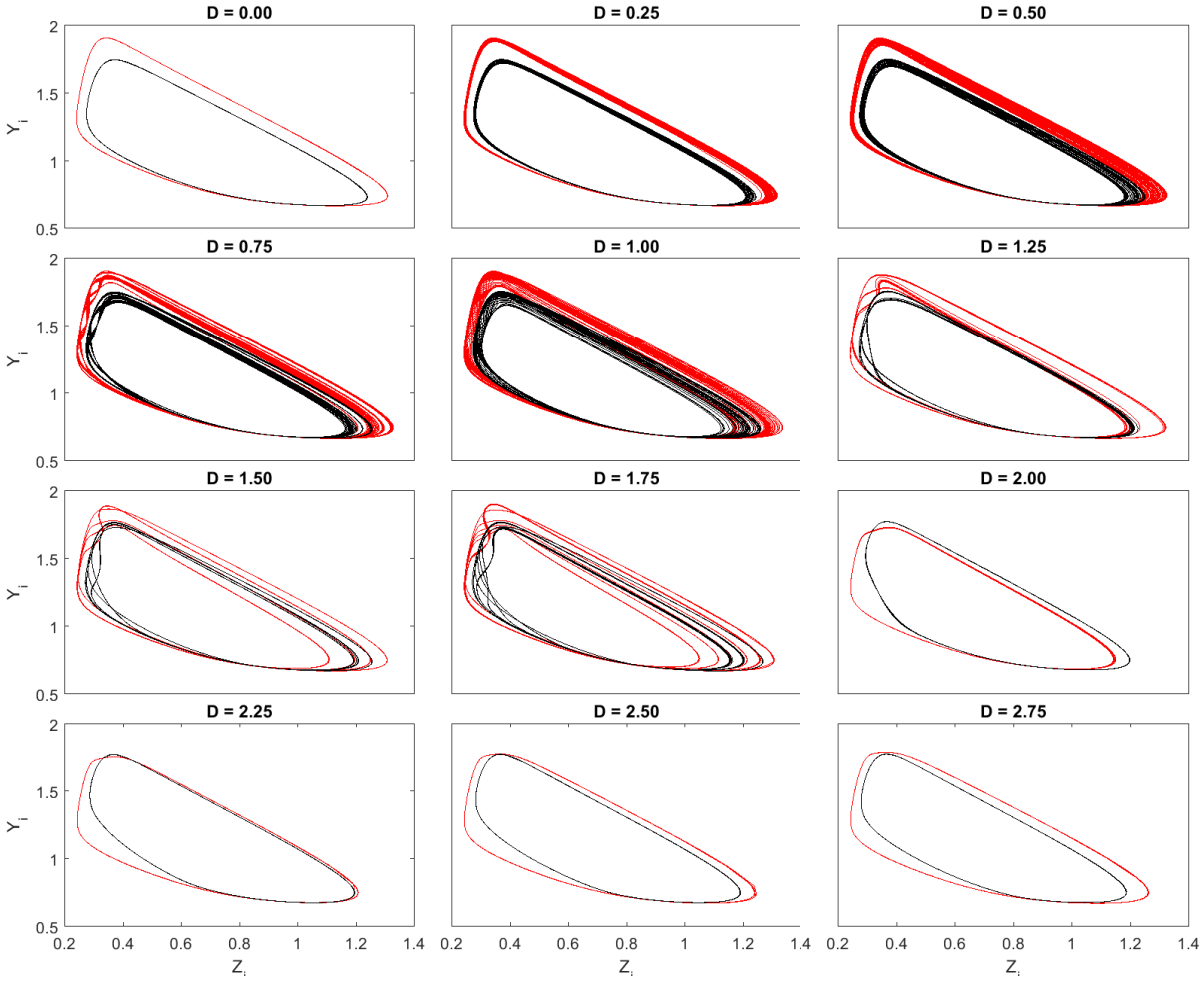

Figure 4: Attractors in the respective (Z, Y) phase space of two oscillatory cells with $\beta_1 = 0.4$ (red) and $\beta_2 = 0.5$ (black), for various values of the coupling strength D. Each panel shows a single trajectory plotted for $5 \leq t \leq 50$ to ensure that transient behaviour is discarded and only long-term dynamics are shown. The initial condition is $(Z_1, Y_1, Z_2, Y_2) = (1.5, 0.5, 1.0, 0.8)$ in all cases, but different initial conditions produce identical graphs. Other parameter values as shown in Table 1.

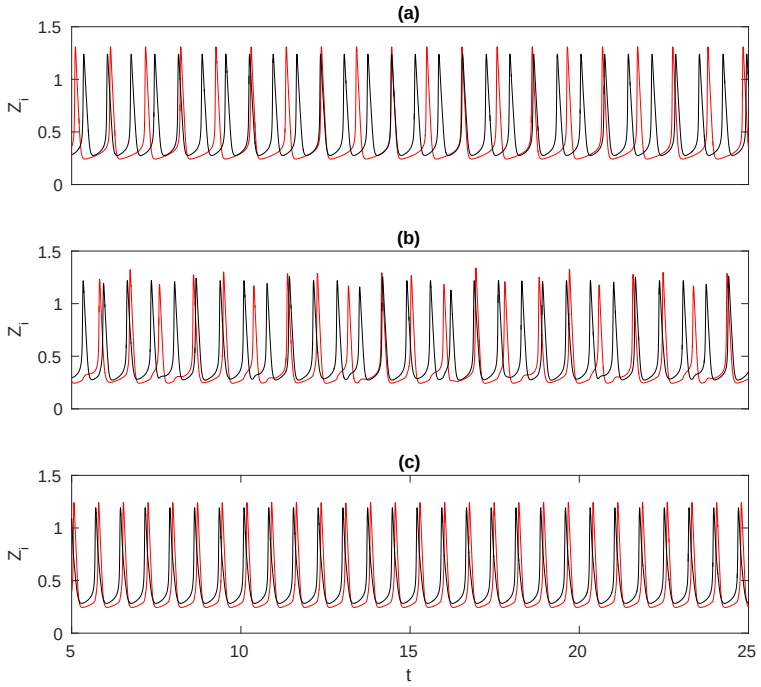

Figure 5: Time series for cytosolic Ca^{2+} concentration Z_i for two oscillatory cells with $\beta_1 = 0.4$ (red) and $\beta_2 = 0.5$ (black) for three coupling strengths: (a) $D = 0$, the cells are uncoupled and oscillate independently; (b) $D = 1$, the cells oscillate asynchronously and with variable amplitude; (c) $D = 2.5$, the cells are synchronised with a phase lag. Each solution is plotted for $5 \leq t \leq 25$ to ensure that transient behaviour is discarded and only long-term dynamics are shown. The initial condition is $(Z_1, Y_1, Z_2, Y_2) = (1.5, 0.5, 1.0, 0.8)$ in all cases, but different initial conditions produce identical graphs. Other parameter values as shown in Table 1.

considered here (results not shown). The attractors shown in Fig. 8 are insensitive to a range of initial conditions suggesting that there is no bistability.

Viewing the dynamics as time series or in phase space offers little insight into the changing frequencies of oscillation as the coupling strength increases and the cells approach synchronisation. We therefore examine the power spectrum of each cell's cytosolic Ca^{2+} concentration $Z_i(t)$, which decomposes the time series into a distribution of sinusoidal functions with different frequencies. The power P_i of a given frequency ω is defined as

$$P_i(\omega) = \left| \int_0^T Z_i(t) e^{-i\omega t} dt \right|^2 . \tag{19}$$

This was calculated using Matlab's *fft* function. The power spectrum provides an additional means of analysing the change in behaviour as the coupling strength D increases.

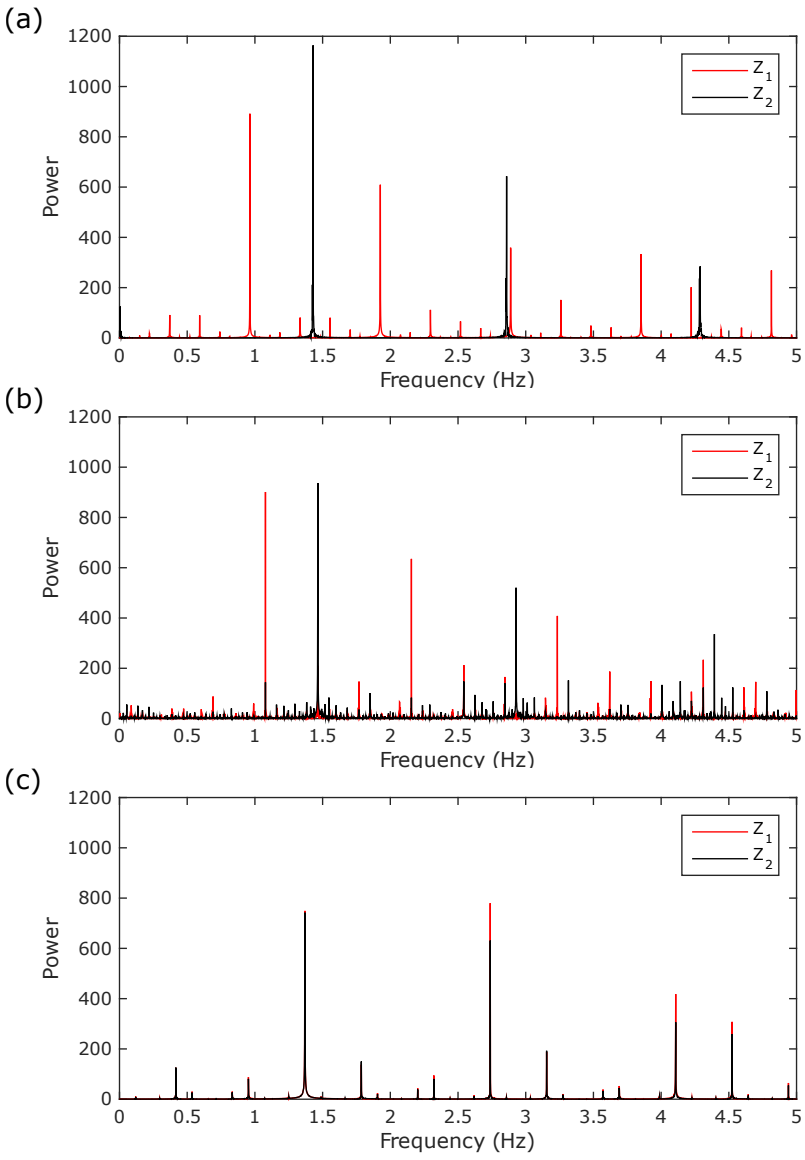

Figure 6: Power spectra of the time series shown in Fig. 5 for two oscillatory cells with $\beta_1 = 0.4$ (red), $\beta_2 = 0.5$ (black), for the same three different coupling strengths D: (a) $D = 0$, the cells are uncoupled and oscillate independently; (b) $D = 1$, the cells oscillate asynchronously and with variable amplitude; (c) $D = 2.5$, the cells are synchronised and share a common set of frequencies. Power spectra are computed according to Eq. (19). Other parameter values as shown in Table 1.

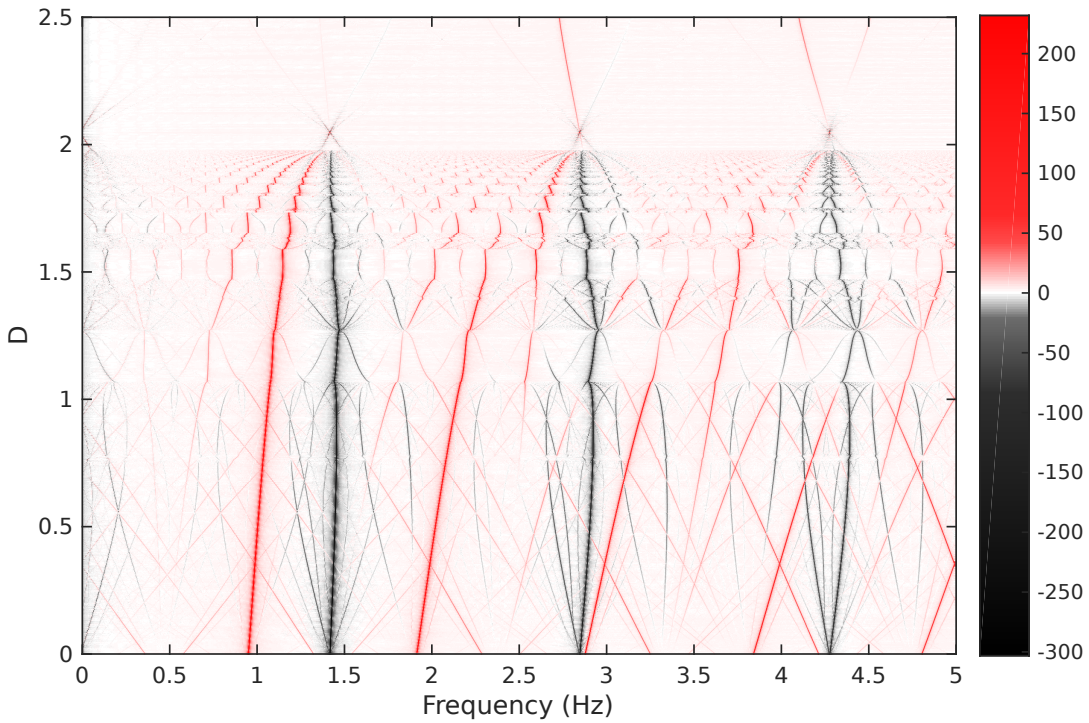

Figure 7: The difference in power spectra (cell 1 minus cell 2) between two oscillatory cells with $\beta_1 = 0.4$ and $\beta_2 = 0.5$, as a function of coupling strength D. Red indicates frequencies at which cell 1 has higher power; black indicates frequencies at which cell 2 has higher power. The cells synchronise when the frequencies coalesce at around $D = 2$. Other parameter values as shown in Table 1.

Figure 6 shows the power spectra of each cell at the same three coupling strengths as shown in Fig. 5. When the cells are uncoupled ($D = 0$), their respective power spectra are independent (Fig. 6(a)). When the cells are coupled with $D = 1$, the two power spectra are irregular, indicating that the cells are exhibiting complex behaviour composed of multiple frequencies (Fig. 6(b)). When the coupling is sufficiently strong ($D = 2.5$), the two power spectra are almost identical, with differences only in the magnitude of the power (Fig. 6(c)). This indicates that the cells have become synchronised.

Since both the trajectories and the frequency distributions of the cells qualitatively change as the coupling increases, we expect some form of bifurcation to occur in the frequency domain when the cells synchronise. To better understand the dynamics in the approach to synchronisation, we plot the difference in power spectra (power for cell 1 minus power for

cells 2) as a function of coupling strength D (Fig. 7). The colour represents the difference in power between the cells, with red representing the frequencies at which cell 1 has greater power and black representing the frequencies at which cell 2 has greater power. At $D = 0$, there are pairs of points in black and red, indicating the independent frequencies of the two uncoupled cells. As the coupling strength increases additional frequencies are introduced, corresponding to the amplitude-modulated oscillations seen in Fig. 5. These frequencies are gradually drawn closer together as the coupling strength increases. At approximately $D = 2$, groups of frequencies coalesce into a primary common frequency of around 1.4 Hz, together with higher harmonics. This corresponds to synchronisation of the cells.

3.3. Coupling an oscillatory and an excitable cell

We now examine the dynamics of an excitable cell ($\beta_1 = 0.25$) coupled to an oscillatory cell ($\beta_2 = 0.35$). The attractors for each cell are shown in Figure 8 for a range of coupling strengths D. When weakly coupled ($D \leq 0.5$ in Fig. 8), the small flux of Ca^{2+} between the cells causes the excitable cell to oscillate with small amplitude, but this perturbation does not reach the threshold required for a large-amplitude Ca^{2+} spike. When the coupling strength is higher ($D \geq 0.75$ in Fig. 8), the Ca^{2+} flux into the excitable cell is large enough to push its Ca^{2+} concentration beyond the excitation threshold. As a consequence, the trajectory of the excitable cell makes a large excursion in phase space, in the form of a large-amplitude Ca^{2+} oscillation. At certain coupling strengths (e.g. $D = 2.0$, $D = 2.25$ in Fig. 8), the excitable cell undergoes a mixture of small- and large-amplitude oscillations, i.e. a mixed-mode oscillation. Eventually, when the coupling strength is sufficiently high ($D \geq 2.5$ in Fig. 8), these mixed-mode oscillations cease and the cells synchronise. The attractors shown in Fig. 8 are insensitive to a range of initial conditions suggesting that there is no bistability.

Figure 9 shows the amplitude of the oscillations as D increases. This reveals the threshold value of the coupling strength ($D \approx 0.55$) required to produce a large-amplitude Ca^{2+} spike in the excitable cell. It also shows that following synchronisation ($D \geq 2.25$), there is a sudden drop in the amplitude in the excitable cell, but not in the oscillatory cell.

To analyse the dynamics in the approach to synchrony, we plot the difference in the

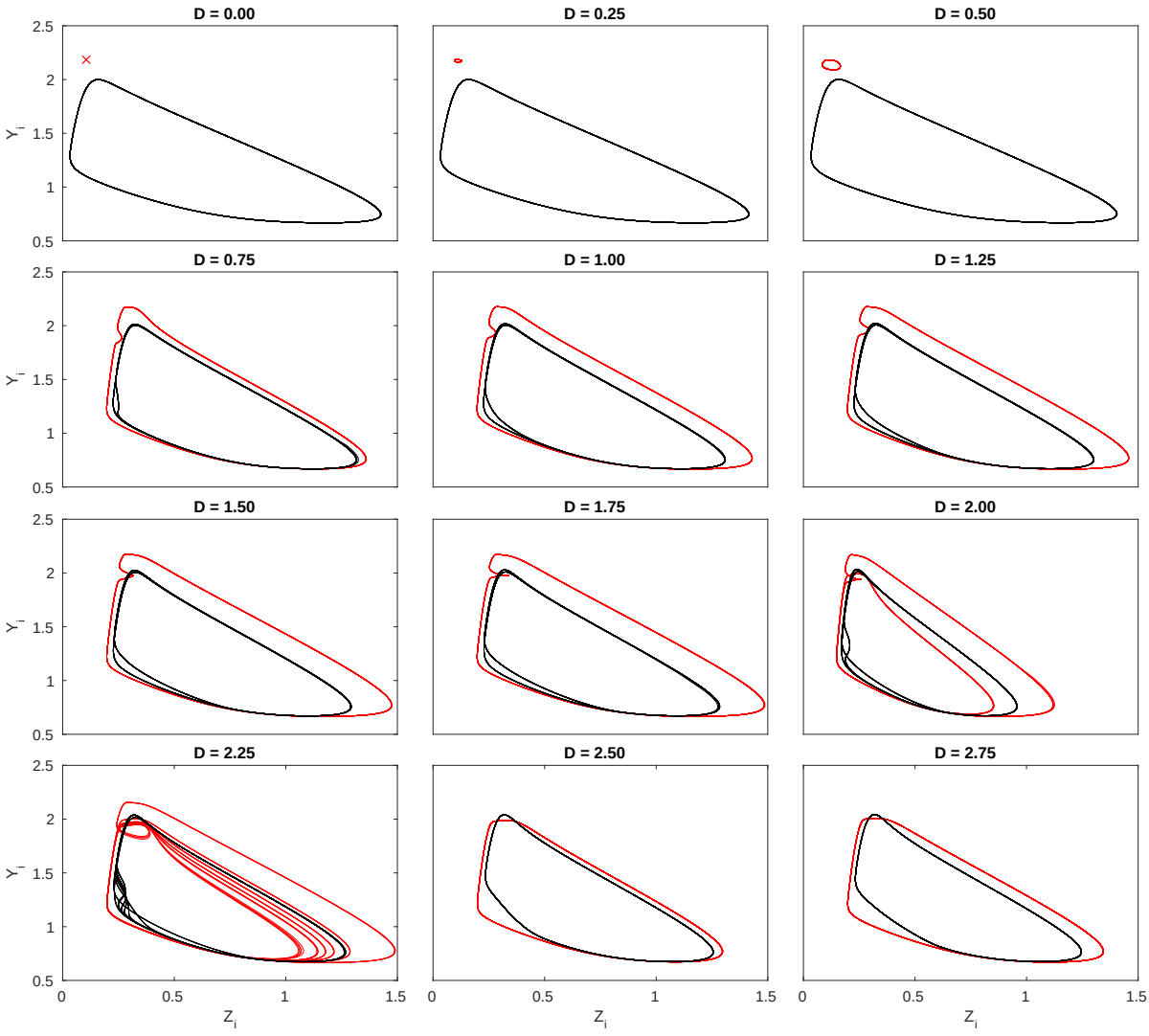

Figure 8: Attractors in the respective (Z, Y) phase space of an excitable cell with $\beta_1 = 0.25$ (red) coupled to an oscillatory cell with $\beta_2 = 0.35$ (black), for various values of the coupling strength D. When $D = 0$, cell 1 has a stable steady state (red cross). When the coupling strength D is sufficiently high ($D \geq 0.75$), the flux of Ca^{2+} from the oscillatory cell to the excitable cell is enough to exceed the excitation threshold, causing the excitable cell to oscillate with large amplitude. Both cells then exhibit amplitude-modulated oscillations, before eventually synchronising. Each panel shows a single trajectory plotted for $5 \leq t \leq 50$ to ensure that transient behaviour is discarded and only long-term dynamics are shown. The initial condition is $(Z_1, Y_1, Z_2, Y_2) = (1.5, 0.5, 1.0, 0.8)$ in all cases, but different initial conditions produce identical graphs. Other parameter values as shown in Table 1.

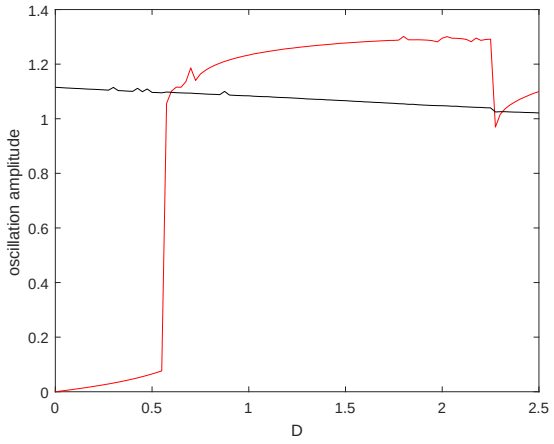

Figure 9: Amplitude of oscillations in an excitable cell with $\beta_1 = 0.25$ (red) coupled to an oscillatory cell with $\beta_2 = 0.35$ (black) for varying coupling strength D. Amplitude is measured as the difference between the minimum and maximum values of $Z_i(t)$ on the attractor. For $D < 0.55$, the excitable cell undergoes sub-threshold oscillations as coupling is insufficient to produce a Ca^{2+} spike. For $0.55 < D < 2.25$, coupling induces large-amplitude oscillations in the excitable cell and the cells oscillate asynchronously. For $D > 2.25$, the cells are synchronised. Other parameter values as shown in Table 1.

power spectra of the cytosolic Ca^{2+} concentration Z_i for the two cells (cell 1 minus cell 2), shown in Figure 10. For relatively weak coupling ($D < 0.55$), the frequency distributions of both cells are the same, but the oscillatory cell (cell 2) has greater power indicated by the black lines. This indicates that both cells are oscillating with the same frequency, but cell 2 has larger amplitude. This corresponds to the excitable cell receiving a stimulus that is below the excitation threshold, as seen in Fig. 9. At around $D = 0.55$, the excitable cell (cell 1) switches from a small-amplitude, sub-threshold oscillation to a limit cycle consisting of a large-amplitude oscillation followed by a small-amplitude oscillation. As D approaches approximately 0.72, the excitable cell undergoes a complex transition, eventually resulting in a large-amplitude oscillation at a single dominant frequency around half the natural frequency of the oscillatory cell. As coupling strength increases up to $D = 2$, there is little further change in the power spectra of each cell. At $D = 2$, additional frequencies are introduced to the excitable cell's oscillations in an apparent period-doubling cascade. These frequencies coalesce with those of the oscillatory cell at around $D = 2.25$, leaving a simple limit cycle where the cells are synchronised and oscillate with a common frequency.

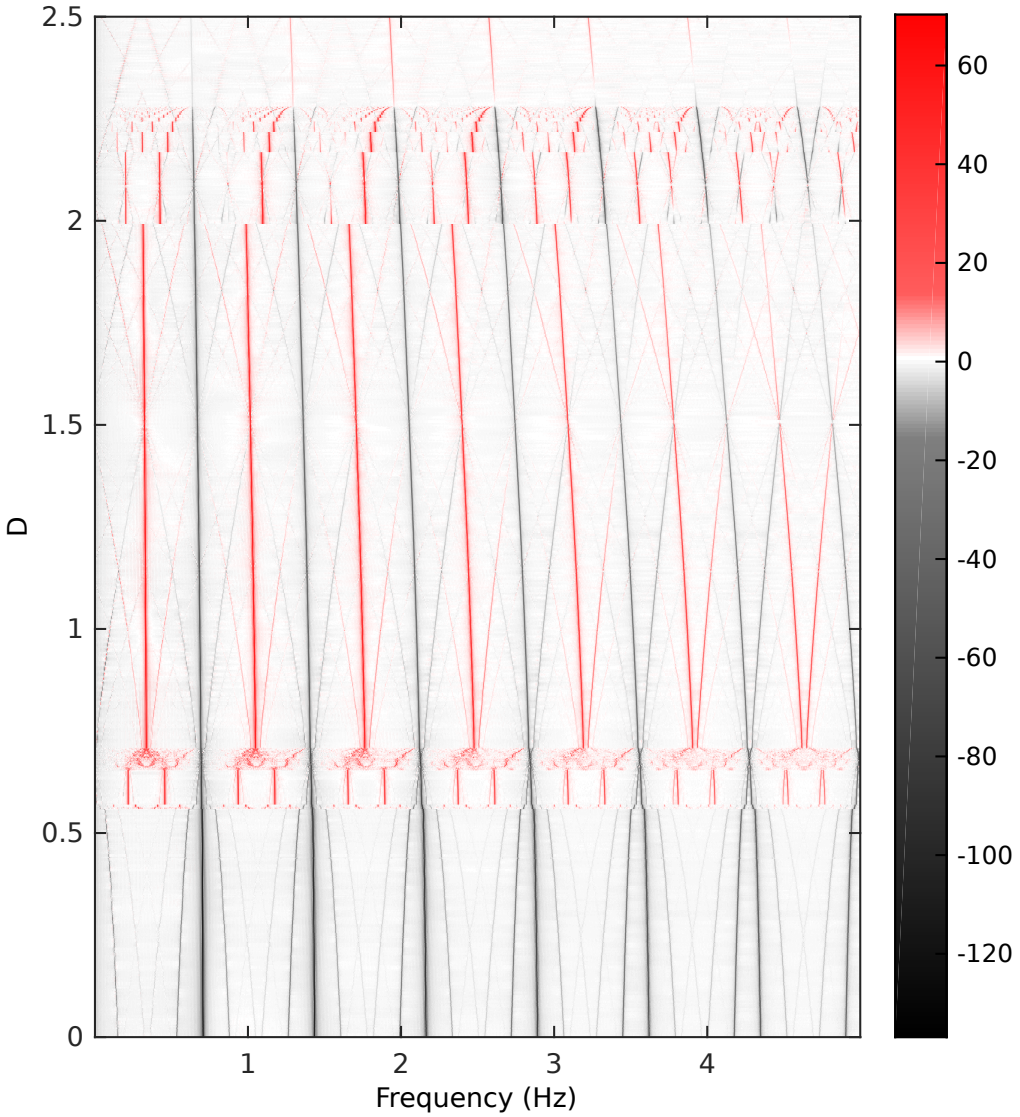

Figure 10: The difference in power spectra (cell 1 minus cell 2) between an excitable cell with $\beta_1 = 0.25$ and an oscillatory cell with $\beta_2 = 0.35$, as a function of coupling strength D. Red indicates frequencies at which cell 1 has higher power; black indicates frequencies at which cell 2 has higher power. The cells synchronise when the frequencies coalesce at around $D = 2.25$. Other parameter values as shown in Table 1.

4. Discussion

We have studied the dynamics of Ca^{2+} within a system of two coupled cells using a minimal Ca^{2+} model [24], which is based on Ca^{2+}-induced Ca^{2+} release. This model can produce either excitable or oscillatory dynamics depending on the strength of external stimulation to the IP_3-mediated Ca^{2+} release pathway. We extended the model to two adjacent, coupled cells via a linear coupling term representing Ca^{2+} flux between the cells via gap junctions. We investigated the dynamics of the coupled system when the cells had different values of the bifurcation parameter, and across a range of coupling strengths.

The dynamics of coupled cells described by different parameter values is physiologically relevant because cells can exhibit spatial variation in behaviour. This can arise as a consequence of a spatial concentration gradient in some exogenous signalling factor. An example is the blood-borne mediator ATP, which modulates the production of IP_3, and which varies spatially depending on the blood vessel wall shear stress [56, 57]. Cells can also exhibit intrinsic heterogeneities in their response to stimuli [58].

When two heterogeneous oscillatory cells are coupled, they exhibit amplitude-modulated oscillations and their frequencies are drawn together as the coupling strength increases. When an oscillatory cell is coupled weakly to an excitable cell, the excitable cell undergoes sub-threshold oscillations. As the coupling strength increases above a critical level, the excitable cell starts to undergo large-amplitude oscillations, which can include mixed-mode oscillations.

When the coupling strength is sufficiently high (i.e. gap junctions permit rapid transport of Ca^{2+} between the two cell cytosols), the cells become synchronised. This is consistent with results from a previous study [10], which modelled Ca^{2+} oscillations in heterogeneous hepatocytes coupled via Ca^{2+} gap junctions. In addition, our results show that strongly coupled cells exhibit the same dynamics (either excitable or oscillatory) as a single cell with the average of two coupled cells' parameter values. Our spectral analysis is not a mathematically rigorous characterisation of the synchronisation of two heterogeneous oscillators. Nevertheless, it does gives insight into the complex dynamics that occur in the approach to

synchrony. As cells are coupled increasingly strongly their frequencies are drawn gradually closer together until they coalesce. However, in some cases there are additional frequency bifurcations as coupling strength increases, including apparent period-doubling cascades.

Synchronisation of the coupled cell system (i.e. phase-lagged oscillation with a common frequency) occurs at a dimensionless coupling strength D between 2 and 2.5 in the cases studied (Figs. 7 and 10). However, there are still differences in amplitude and phase between the two oscillating cells following synchronisation. Much stronger coupling is required to eliminate these differences. This is consistent with the very strong coupling required to bring the steady state of the coupled system close to that of the averaged single cell model (Fig. 3). The coupling strength required for either in-phase synchrony or equalisation of steady states corresponds to a Ca^{2+} diffusion coefficient that is comparable to experimental estimates from extracellular free Ca^{2+} diffusion. The coupling between adjacent cells via gap junctions is likely to correspond to much smaller values for the coupling strength. Hence, complete equalisation of adjacent cells is unlikely under the model considered, and either amplitude-modulated oscillations, or phase-lagged synchronisation is more likely.

Our results show that the movement of calcium between two cells can lead to behaviour that is fundamentally different from what one would predict from looking at either cell in isolation. This is particularly true when two oscillatory cells with different frequencies are coupled, or an oscillatory cell is coupled to an excitable cell. We have shown this phenomenon using a very simple model of intracellular Ca^{2+} dynamics. The analytical results we have given for coupled cells are specific to this simple model, particularly the assumption that the rate of change of cytosolic calcium is linear in the bifurcation parameter. More sophisticated models include more chemical species, ion channels, and membrane potential [16, 30, 59]. Many of these models contain a similar bifurcation structure to the model we have studied [24], with Hopf bifurcations separating a region of oscillatory dynamics from stable regions, e.g. [16, 23, 59–61]. Despite the simplicity of the model we have used, we conjecture that some of the qualitative behaviour we have demonstrated, for example amplitude-modulated oscillations and coalescence of frequencies, will also occur in more sophisticated models.

An additional limitation of our model is the assumption of a linear coupling term, corresponding to Fick's law, for the transport of Ca^{2+} from high to low concentration. In reality, movement of charged ions is governed by a combination of concentration gradient and membrane potential. This can be modelled by more complex coupling mechanisms, such as the GHK electrodiffusion equation [21]. An example of this coupling mechanism has been used to model the flow of ions (specifically Ca^{2+}, K^+, Na^+ and Cl^-) between two cells [48]. A similar coupling expression could be applied to examine whether a more accurate and complex coupling term would affect the underlying dynamics of the system. Deterministic models such as these rely on average concentrations of ions such as Ca^{2+}, but it is increasingly recognised that stochasticity can significantly affect the dynamics due to relatively small numbers of individual ions [31, 32]. This can be a major driver of the macroscale patterns that emerge from cell coupling [62, 63].

Real cells do not occur in pairs but in large populations, with an irregular spatial structure. These can be modelled as a continuum of oscillators [42, 43], regular grids forming a tissue slice [59, 64, 65] or as general network topologies [66, 67]. Nevertheless, our approach provides a framework that can aid in the understanding of complex calcium dynamics that can occur in multiple, coupled, heterogeneous cells.

References

[1] K. A. Dora, M. P. Doyle, B. R. Duling, Elevation of intracellular calcium in smooth muscle causes endothelial cell generation of NO in arterioles, Proceedings of the National Academy of Sciences 94 (12) (1997) 6529–6534.

[2] M. J. Berridge, P. Lipp, M. D. Bootman, The versatility and universality of calcium signalling, Nature Reviews Molecular Cell Biology 1 (1) (2000) 11–21.

[3] G. Dupont, J. Sneyd, Recent developments in models of calcium signalling, Current Opinion in Systems Biology 3 (2017) 15–22.

[4] M. Wilkins, J. Sneyd, Intercellular spiral waves of calcium, Journal of Theoretical Biology 191 (3) (1998) 299–308.

[5] S. Schuster, M. Marhl, T. Höfer, Modelling of simple and complex calcium oscillations, The FEBS Journal 269 (5) (2002) 1333–1355.

[6] F. Liu, R. Zhou, H. Yan, H. Yin, X. Wu, Y. Tan, L. Li, Metabotropic glutamate receptor 5 modulates calcium oscillation and innate immune response induced by lipopolysaccharide in microglial cell, Neuroscience 281 (2014) 24–34.

[7] R. Balaji, C. Bielmeier, H. Harz, J. Bates, C. Stadler, A. Hildebrand, A.-K. Classen, Calcium spikes, waves and oscillations in a large, patterned epithelial tissue, Scientific Reports 7 (2017) 42786.

[8] G. Dupont, L. Combettes, G. S. Bird, J. W. Putney, M. Brini, Calcium oscillations, Cold Spring Harbor Perspectives in Biology 3 (3) (2011) a004226.

[9] E. A. Eugenín, H. González, C. G. Sáez, J. C. Sáez, Gap junctional communication coordinates vasopressin-induced glycogenolysis in rat hepatocytes, American Journal of Physiology-Gastrointestinal and Liver Physiology 274 (6) (1998) G1109–G1116.

[10] T. Höfer, Model of intercellular calcium oscillations in hepatocytes: synchronization of heterogeneous cells, Biophysical Journal 77 (3) (1999) 1244–1256.

[11] M. J. Sanderson, Intercellular calcium waves mediated by inositol triphosphate, Wiley, Chicester, UK, 1995.

[12] C. Giaume, L. Venance, Intercellular calcium signaling and gap junctional communication in astrocytes, Glia 24 (1) (1998) 50–64.

[13] R. K. Benninger, M. Zhang, W. S. Head, L. S. Satin, D. W. Piston, Gap junction coupling and calcium waves in the pancreatic islet, Biophysical Journal 95 (11) (2008) 5048–5061.

[14] D. I. Yule, E. Stuenkel, J. A. Williams, Intercellular calcium waves in rat pancreatic acini: mechanism of transmission, American Journal of Physiology-Cell Physiology 271 (4) (1996) C1285–C1294.

[15] T. Hassinger, P. Guthrie, P. Atkinson, M. Bennett, S. Kater, An extracellular signaling component in propagation of astrocytic calcium waves, Proceedings of the National Academy of Sciences 93 (23) (1996) 13268–13273.

[16] M. Koenigsberger, R. Sauser, J. L. Bény, J. J. Meister, Role of the endothelium on arterial vasomotion, Biophysical Journal 88 (6) (2005) 3845–3854.

[17] P. Cao, X. Tan, G. Donovan, M. J. Sanderson, J. Sneyd, A Deterministic Model Predicts the Properties of Stochastic Calcium Oscillations in Airway Smooth Muscle Cells, PLOS Computational Biology 10 (8) (2014) 1–15.

[18] J.-J. Meister, J. C. Quijano, Ultrafast Calcium Wave in Cultured Vascular Smooth Muscle Cells, Biophysical Journal 106 (2) (2017) 321a–322a.

[19] R. E. Haddock, C. E. Hill, Rhythmicity in arterial smooth muscle, Journal of Physiology 566 (3) (2005) 645–656.

[20] D. Seppey, R. Sauser, M. Koenigsberger, J.-L. Bény, J.-J. Meister, Intercellular calcium waves are associated with the propagation of vasomotion along arterial strips, American Journal of Physiology-Heart and Circulatory Physiology 298 (2) (2010) H488—-H496.

[21] S. Nagaraja, A. Kapela, N. M. Tsoukias, Intercellular communication in the vascular wall: A modeling perspective, Microcirculation 19 (5) (2012) 391–402.

[22] H. Girouard, C. Iadecola, Neurovascular coupling in the normal brain and in hypertension, stroke, and Alzheimer disease, Journal of Applied Physiology 100 (1) (2006) 328–335.

[23] T. Meyer, L. Stryer, Molecular model for receptor-stimulated calcium spiking, Proceedings of the National Academy of Sciences 85 (July) (1988) 5051–5055.

[24] A. Goldbeter, G. Dupont, M. J. Berridge, Minimal model for signal-induced Ca2+ oscillations and for their frequency encoding through protein phosphorylation, Proceedings of the National Academy of Sciences 87 (4) (1990) 1461–1465.

[25] G. Dupont, A. Goldbeter, One-pool model for Ca2+ oscillations involving Ca2+ and inositol 1, 4, 5-trisphosphate as co-agonists for Ca2+ release, Cell Calcium 14 (4) (1993) 311–322.

[26] A. Atri, J. Amundson, D. Clapham, J. Sneyd, A single-pool model for intracellular calcium oscillations and waves in the Xenopus laevis oocyte, Biophysical Journal 65 (4) (1993) 1727–1739.

[27] Y.-X. Li, J. Rinzel, Equations for InsP3 receptor-mediated [Ca2+]i oscillations derived from a detailed kinetic model: a Hodgkin-Huxley like formalism, Journal of Theoretical Biology 166 (4) (1994) 461–473.

[28] R. Somogyi, J. Stucki, Hormone-induced calcium oscillations in liver cells can be explained by a simple one pool model., Journal of Biological Chemistry 266 (17) (1991) 11068–11077.

[29] G. W. De Young, J. Keizer, A single-pool inositol 1, 4, 5-trisphosphate-receptor-based model for agonist-stimulated oscillations in Ca2+ concentration, Proceedings of the National Academy of Sciences 89 (20) (1992) 9895–9899.

[30] D. Parthimos, D. H. Edwards, T. M. Griffith, Minimal model of arterial chaos generated by coupled intracellular and membrane Ca2+ oscillators, American Journal of Physiology 277 (3) (1999) H1119–H1144.

[31] M. Perc, A. K. Green, C. J. Dixon, M. Marhl, Establishing the stochastic nature of intracellular calcium oscillations from experimental data, Biophysical Chemistry 132 (1) (2008) 33–38.

[32] M. Perc, M. Rupnik, M. Gosak, M. Marhl, Prevalence of stochasticity in experimentally observed responses of pancreatic acinar cells to acetylcholine, Chaos: An Interdisciplinary Journal of Nonlinear Science 19 (3) (2009) 037113.

[33] G. B. Ermentrout, D. H. Terman, Mathematical Foundations of Neuroscience, Springer, 2010.

[34] M. Perc, M. Marhl, Different types of bursting calcium oscillations in non-excitable cells, Chaos, Solitons & Fractals 18 (4) (2003) 759–773.

[35] C. Morris, H. Lecar, Voltage oscillations in the barnacle giant muscle fiber, Biophysical Journal 35 (1) (1981) 193–213.

[36] N. Kopell, G. B. Ermentrout, Mechanisms of phase-locking and frequency control in pairs of coupled neural oscillators, in: B. Fiedler (Ed.), Handbook of Dynamical Systems, Vol. 2, Elsevier, 2002, pp. 3–54.

[37] M. Perc, M. Marhl, Local dissipation and coupling properties of cellular oscillators: a case study on calcium oscillations, Bioelectrochemistry 62 (1) (2004) 1–10.

[38] M. Perc, M. Marhl, Synchronization of regular and chaotic oscillations: The role of local divergence and the slow passage effecta case study on calcium oscillations, International Journal of Bifurcation and Chaos 14 (08) (2004) 2735–2751.

[39] J. Quan-Bao, L. Qi-Shao, Y. Zhuo-Qin, D. Li-Xia, Bursting Ca2+ oscillations and synchronization in coupled cells, Chinese Physics Letters 25 (11) (2008) 3879.

[40] M. S. Imtiaz, P.-Y. von der Weid, D. F. van Helden, Synchronization of Ca2+ oscillations: a coupled oscillator-based mechanism in smooth muscle, The FEBS journal 277 (2) (2010) 278–285.

[41] M. J. Alam, L. Bhayana, G. R. Devi, H. D. Singh, R. B. Singh, B. I. Sharma, Intercellular synchronization of diffusively coupled Ca2+ oscillators, Journal of Chemical Biology 5 (1) (2012) 27–34.

[42] N. Kopell, G. Ermentrout, Symmetry and phaselocking in chains of weakly coupled oscillators, Communications on Pure and Applied Mathematics 39 (5) (1986) 623–660.

[43] G. B. Ermentrout, Oscillator death in populations of "all to all" coupled nonlinear oscillators, Physica D: Nonlinear Phenomena 41 (2) (1990) 219–231.

[44] G. B. Ermentrout, N. Kopell, Multiple pulse interactions and averaging in systems of coupled neural oscillators, Journal of Mathematical Biology 29 (3) (1991) 195–217.

[45] B. Ermentrout, M. Pascal, B. Gutkin, The effects of spike frequency adaptation and negative feedback on the synchronization of neural oscillators, Neural Computation 13 (6) (2001) 1285–1310.

[46] J. A. Filosa, A. D. Bonev, M. T. Nelson, Calcium dynamics in cortical astrocytes and arterioles during neurovascular coupling, Circulation Research 95 (10) (2004) e73–e81.

[47] M. Bindschadler, J. Sneyd, A bifurcation analysis of two coupled calcium oscillators, Chaos 11 (1) (2001) 237–246.

[48] A. Kapela, A. Bezerianos, N. M. Tsoukias, A mathematical model of Ca2+ dynamics in rat mesenteric smooth muscle cell: Agonist and NO stimulation, Journal of Theoretical Biology 253 (2) (2008) 238–260.

[49] V. Verselis, R. L. White, D. C. Spray, M. V. L. Bennett, Gap junctional conductance and permeability are linearly related, Science 234 (1986) 461–465.

[50] A. Sherman, J. Rinzel, Model for synchronization of pancreatic beta-cells by gap junction coupling, Biophysical Journal 59 (3) (1991) 547–559.

[51] T. Höfer, A. Politi, R. Heinrich, Intercellular Ca2+ wave propagation through gap-junctional Ca2+ diffusion: a theoretical study, Biophysical Journal 80 (1) (2001) 75–87.

[52] E. A. Codling, M. J. Plank, S. Benhamou, Random walk models in biology, Journal of the Royal Society Interface 5 (25) (2008) 813–834.

[53] S. Hrabětová, D. Masri, L. Tao, F. Xiao, C. Nicholson, Calcium diffusion enhanced after cleavage of negatively charged components of brain extracellular matrix by chondroitinase ABC, Journal of Physiology 587 (16) (2009) 4029–4049.

[54] A. Tonnelier, Threshold curve for the excitability of bidimensional spiking neurons, Physical Review E 90 (2) (2014) 022701.

[55] J. Burke, M. Desroches, A. M. Barry, T. J. Kaper, M. A. Kramer, A showcase of torus canards in neuronal bursters, Journal of Mathematical Neuroscience 2 (1) (2012) 3.

[56] Q.-K. Tran, K. Ohashi, H. Watanabe, Calcium signalling in endothelial cells, Cardiovascular Research 48 (1) (2000) 13–22.

[57] K. Dormanns, E. M. J. van Disseldorp, R. G. Brown, T. David, Neurovascular coupling and the influence of luminal agonists via the endothelium, Journal of Theoretical Biology 364 (2015) 49–70.

[58] S. D. Burton, G. B. Ermentrout, N. N. Urban, Intrinsic heterogeneity in oscillatory dynamics limits correlation-induced neural synchronization, Journal of Neurophysiology 108 (8) (2012) 2115–2133.

[59] K. Dormanns, R. G. Brown, T. David, The role of nitric oxide in neurovascular coupling, Journal of Theoretical Biology 394 (2016) 1–17.

[60] J. M. Gonzalez-Fernandez, B. Ermentrout, On the origin and dynamics of the vasomotion of small arteries, Mathematical Biosciences 119 (2) (1994) 127–167.

[61] J. P. Johny, M. J. Plank, T. David, Importance of altered levels of SERCA, IP_3R, and RyR in vascular smooth muscle cell, Biophysical Journal 112 (2) (2017) 265–287.

[62] M. Perc, M. Gosak, M. Marhl, Periodic calcium waves in coupled cells induced by internal noise, Chemical Physics Letters 437 (1-3) (2007) 143–147.

[63] M. Gosak, M. Marhl, M. Perc, Chaos out of internal noise in the collective dynamics of diffusively coupled cells, European Physical Journal B 62 (2) (2008) 171–177.

[64] M. Gosak, A. Stozer, R. Markovic, J. Dolensek, M. Perc, M. Slak Rupnik, M. Marhl, Critical and supercritical spatiotemporal calcium dynamics in beta cells, Frontiers in Physiology 8 (2017) 1106.

[65] A. Kenny, C. Zakkaroff, M. J. Plank, T. David, Massively parallel simulations of neurovascular coupling with extracellular diffusion, Journal of Computational Science.

[66] J. Kozloski, Automated reconstruction of neural tissue and the role of large-scale simulation, Neuroinformatics 9 (2-3) (2011) 133–142.

[67] M. Gosak, A. Stožer, R. Markovič, J. Dolenšek, M. Marhl, M. Slak Rupnik, M. Perc, The relationship between node degree and dissipation rate in networks of diffusively coupled oscillators and its significance for pancreatic beta cells, Chaos: An Interdisciplinary Journal of Nonlinear Science 25 (7) (2015) 073115.